Journal of Inorganic Biochemistry 167 (2017) 60–67

Contents lists available at ScienceDirect

Journal of Inorganic Biochemistry

journal homepage: www.elsevier.com/locate/jinorgbio

Heterolytic O—O bond cleavage: Functional role of Glu113 during *bis*-Fe(IV) formation in MauG

Jiafeng Geng [a,1], Lu Huo [a,2], Aimin Liu [a,b,*]

[a] Department of Chemistry, Georgia State University, Atlanta, GA 30303, United States
[b] Department of Chemistry, University of Texas at San Antonio, San Antonio, TX 78249, United States

ARTICLE INFO

Article history:
Received 6 July 2016
Received in revised form 23 September 2016
Accepted 8 November 2016
Available online 9 November 2016

Keywords:
Cofactor biogenesis
Diheme
Ferryl intermediate
Mixed-valence
Reactive oxygen species
Remote catalysis

ABSTRACT

The diheme enzyme MauG utilizes H_2O_2 to perform oxidative posttranslational modification on a protein substrate. A *bis*-Fe(IV) species of MauG was previously identified as a key intermediate in this reaction. Heterolytic cleavage of the O—O bond of H_2O_2 drives the formation of the *bis*-Fe(IV) intermediate. In this work, we tested a hypothesis that a glutamate residue, Glu113 in the distal pocket of the pentacoordinate heme of MauG, facilitates heterolytic O—O bond cleavage, thereby leading to *bis*-Fe(IV) formation. This hypothesis was proposed based on sequence alignment and structural comparison with other H_2O_2-utilizing hemoenzymes, especially those from the diheme enzyme superfamily that MauG belongs to. Electron paramagnetic resonance (EPR) characterization of the reaction between MauG and H_2O_2 revealed that mutation of Glu113 inhibited heterolytic O—O bond cleavage, in agreement with our hypothesis. This result was further confirmed by the HPLC study in which an analog of H_2O_2, cumene hydroperoxide, was used to probe the pattern of O—O bond cleavage. Together, our data suggest that Glu113 functions as an acid-base catalyst to assist heterolytic O—O bond cleavage during the early stage of the catalytic reaction. This work advances our mechanistic understanding of the H_2O_2-activation process during *bis*-Fe(IV) formation in MauG.

1. Introduction

Hydrogen peroxide (H_2O_2) is produced in a rich array of biological processes, including respiration and peroxisomal β-oxidation [1]. It serves as a transmitter of cellular redox signals [2], while being a biological reactive oxygen species [3]. Although H_2O_2 is a strong oxidant, it is unreactive with most biological molecules because of the high activation energy barrier. Hemoenzymes play an important role in utilizing and detoxifying cellular H_2O_2. There are three major types of H_2O_2-utilizing hemoenzymes: peroxidases, peroxygenases, and catalases (Fig. 1). Notably, the Fe(III) state is the catalytically active form of these enzymes. Unlike most Fe(II)-dependent hemoenzymes, such as cytochrome P450s, which require external electron sources to regenerate the Fe(II) heme from the Fe(III) state at the beginning of each reaction cycle, these H_2O_2-utilizing hemoenzymes work independently and return to the resting Fe(III) state after each turnover [4,5]. As a result, the two oxidizing equivalents from H_2O_2 are both utilized to oxidize the substrate. Although H_2O_2-utilizing hemoenzymes catalyze a wide variety of chemical transformations, a common high-valence heme intermediate, namely compound I, which is an Fe(IV)-oxo species coupled with a porphyrin cation radical, is involved in these enzymatic reactions (Fig. 1) [4,5]. Compound I is generated via heterolytic O—O bond cleavage, which transfers both oxidizing equivalents from H_2O_2 to the protein-bound heme moiety.

In H_2O_2-utilizing hemoenzymes, it is frequently reported that a polar amino acid residue located in the distal heme pocket facilitates the binding and activation of H_2O_2. This residue functions as an acid-base catalyst to promote heterolytic O—O bond cleavage for compound I production (Fig. 1) [6]. Our survey of the literature shows that the most common polar amino acid used in this case is histidine, which is found in the distal heme pocket of catalase [7], peroxidase [8–11], catalase-peroxidase [12], and prostaglandin synthase [13] (Table 1). Another commonly used amino acid is glutamate. The examples include fungal peroxygenase [14,15], chloroperoxidase [16], and bacterial diheme cytochrome *c* peroxidase (bCcP) [17] (Table 1). Interestingly, such polar residues are usually placed in the optimal position for catalysis via an H-bonding interaction with another polar residue or through

Abbreviations: bCcP, bacterial diheme cytochrome *c* peroxidase; EPR, electron paramagnetic resonance; MADH, methylamine dehydrogenase; TTQ, tryptophan tryptophylquinone.

* Corresponding author at: Department of Chemistry, University of Texas at San Antonio, San Antonio, TX 78249-0698, United States.
E-mail address: Feradical@utsa.edu (A. Liu).
[1] Present address: School of Chemistry and Biochemistry, Georgia Institute of Technology, Atlanta, GA.
[2] Present address: Alliance Pharma, Malvern, PA.

http://dx.doi.org/10.1016/j.jinorgbio.2016.11.013
0162-0134/

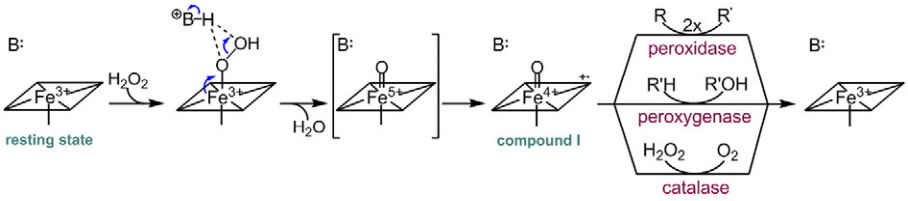

Fig. 1. General reaction mechanism of H_2O_2-utilizing hemoenzymes. "B:" represents the deprotonated state of the acid-base catalytic residue in the distal heme pocket.

a salt bridge with an adjacent charged residue (Table 1). For instance, in *Pseudomonas aeruginosa* bCcP, an asparagine residue forms an H-bonding interaction with the distal glutamate residue [17].

MauG is a diheme enzyme belonging to the bCcP diheme enzyme superfamily. The two ferric hemes in MauG are in different spin states: one is high-spin pentacoordinate with an axial histidine ligand and the other is low-spin hexacoordinate with an axial histidine-tyrosine ligand set (denoted as $Heme_{5C}$ and $Heme_{6C}$, respectively, as shown in (Fig. 2A) [22,24]. MauG catalyzes the final stage of the biosynthesis of a protein-derived redox cofactor, tryptophan tryptophylquinone (TTQ), which functions as the catalytic center of methylamine dehydrogenase (MADH) [25]. During this cofactor biogenesis process, H_2O_2 is utilized as an oxidant to modify two adjacent tryptophan residues of the precursor protein, preMADH, through a radical mechanism (Fig. 2B) [26]. This process is a three-step, six-electron oxidation reaction; each step consumes one equivalent of H_2O_2 and delivers two oxidizing equivalents to preMADH (Fig. 2B) [27,28]. A unique *bis*-Fe(IV) intermediate of MauG, in which $Heme_{5C}$ is present as Fe(IV) = O and $Heme_{6C}$ as Fe(IV) with the axial histidine-tyrosine ligand set retained, is involved in each oxidation step (Fig. 2C) [29–32]. This intermediate is electronically equivalent to compound I, with two oxidizing equivalents above the resting ferric state.

Similar to compound I, the *bis*-Fe(IV) intermediate is generated via heterolytic O—O bond cleavage of H_2O_2. The formation process of *bis*-Fe(IV) is complete within the dead-time of stopped-flow mixing of diferric MauG and H_2O_2 [33], suggesting that the heterolytic O—O bond cleavage is effectively facilitated by the protein matrix in the heme center. Notably, $Heme_{5C}$ is the reactive center that binds and activates H_2O_2 during catalysis, because of its coordination vacancy [34]. A survey of the binding pocket of $Heme_{5C}$ reveals a glutamate residue, Glu113, which is 5.6 Å from the iron ion of $Heme_{5C}$ (Fig. 2A). Previous studies showed that mutation of Glu113 resulted in no detectable TTQ biosynthesis activity from steady-state reactions, but the mutant enzyme achieved partial synthesis of TTQ from *in crystallo* reactions [35]. Herein, we took a closer look at the catalytic role of Glu113 and tested a hypothesis that Glu113 facilitates the activation of H_2O_2 by driving the heterolytic O—O bond cleavage during *bis*-Fe(IV) formation.

2. Experimental

2.1. Reagents

Sodium dithionite (85%), cumene hydroperoxide (80%), cumyl alcohol (97%), acetophenone (99%), and phenethyl alcohol (99%) were purchased from Sigma-Aldrich without further purification. H_2O_2 (30% v/v) was purchased from Fisher Scientific. The concentration of H_2O_2 was determined based on the molar absorptivity of 43.6 M^{-1} cm^{-1} at 240 nm.

2.2. Sequence alignment

Sequence alignment of the bCcP superfamily, including MauG and bCcP from different organisms, was performed using the Molecular Evolutionary Genetics Analysis (MEGA) software. The alignment output was further edited using ESPript [36] for better illustration.

2.3. Protein expression and purification

Recombinant wild-type (WT) MauG and the E113Q mutant were expressed in *Paracoccus denitrificans* and isolated in the periplasmic fraction as described previously [24,35]. The protein concentration was determined using the extinction coefficient of the heme Soret band as described previously [29,35]. All experiments on purified MauG were performed in 50 mM potassium phosphate buffer, pH 7.5.

2.4. Electron paramagnetic resonance (EPR) characterization

EPR experiments were performed using methods described previously [37,38]. Briefly, X-band EPR spectra were recorded in the perpendicular mode on a Bruker ER200D spectrometer coupled with a 4116DM

Table 1
H_2O_2-utilizing hemoenzymes and their corresponding acid-base catalytic residues for heterolytic O—O bond cleavage.

Enzyme	Heme ligand	Acid-base catalyst	Salt-bridge residue	H-bond partner	PDB ID	Ref.
Fatty acid hydroxylase	Cysteine	fatty acid carboxylate group[a]	Arginine	N/A	1IZO	[6,18]
Fungal peroxygenase	Cysteine	Glutamate	Arginine	Threonine[b]	2YP1	[14,15]
Chloroperoxidase	Cysteine	Glutamate	N/A	Histidine	2CPO	[6,16]
Catalase	Tyrosine	Histidine	N/A	Serine	1QQW	[7]
Prostaglandin synthase	Histidine	Histidine	N/A	Threonine	1DIY	[5,13]
KcatG	Histidine	Histidine	N/A	Asparagine	1MWV	[12]
Horseradish peroxidase	Histidine	Histidine	N/A	Asparagine	1ATJ	[6,9]
Cytochrome *c* peroxidase	Histidine	Histidine	N/A	Asparagine	2CYP	[8,11]
Ascorbate peroxidase	Histidine	Histidine	N/A	Asparagine	1APX	[10]
Dye-decolorizing peroxidase (B-type)	Histidine	Arginine	Heme propionate	N/A	3QNR	[19]
Dye-decolorizing peroxidase (D-type)	Histidine	Aspartate	Arginine	N/A	2D3Q	[20,21]
Bacterial di-heme cytochrome *c* peroxidases ($Heme_{5C}$)	Histidine	Glutamate	N/A	Asparagine[c]	2VHD	[17]
MauG ($Heme_{5C}$)	Histidine	Glutamate	N/A	Asparagine	3L4M	[22]
RoxA[d] ($Heme_{5C}$)	Histidine	N/A	N/A	N/A	4B2N	[23]

[a] The carboxylate group belongs to the fatty acid substrate.
[b] The H-bonding interaction between the glutamate residue and the threonine residue is weak.
[c] The asparagine residue is not strictly conserved.
[d] RoxA is an O_2-utilizing enzyme in the bCcP superfamily.

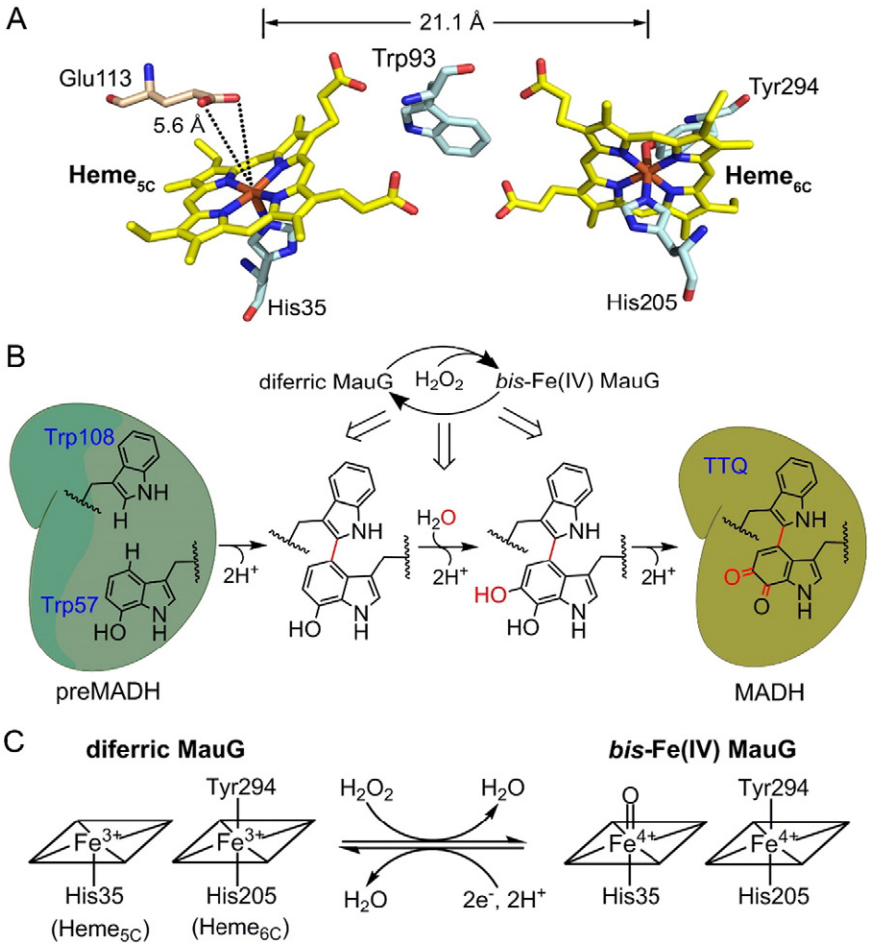

Fig. 2. Diheme enzyme MauG and its catalytic reaction. (A) The diheme cofactor of MauG and the distal Glu113 residue at the $Heme_{5C}$ site (PDB entry: 3L4M). The distance between the carboxylate group of Glu113 and the iron ion of $Heme_{5C}$ is 5.6 Å. The distance between the two heme iron ions is 21.1 Å. A tryptophan residue, Trp93, is located between the hemes and mediates inter-heme electron transfer. (B) The chemical reaction catalyzed by MauG. The *bis*-Fe(IV) intermediate of MauG is involved in all three two-electron oxidation steps of the reaction. Posttranslational modifications on the two tryptophan residues of preMADH are shown in red. H_2O_2 serves as a co-substrate to provide oxidizing equivalents. (C) Chemical conversion between diferric and *bis*-Fe(IV) MauG.

resonator at 100 kHz modulation frequency. The measurement temperature was maintained at 10 K using an ESR910 liquid helium cryostat and an ITC503 temperature controller from Oxford Instruments (Concord, MA). The protein concentration of each EPR sample was 200 μM. The sample volume of each EPR sample was 200 μL. The dithionite-treated samples were prepared by adding ten equivalent of dithionite (from a 20-mM stock solution) to the diferric enzyme. After 10 min incubation, the samples were transferred into EPR tubes via a syringe and flash-frozen in liquid nitrogen. The elapsed time of the freezing process was estimated to be less than 10 s. The H_2O_2-treated samples were prepared by adding one equivalent of H_2O_2 (from a 2-mM stock solution) to the diferric enzyme. After vigorous hand-mixing, the samples were quickly transferred into EPR tubes via a syringe and then flash-frozen in liquid nitrogen. The total sample handling time prior to the freezing process was estimated to be 20–30 s. All EPR measurements were performed in triplicate.

2.5. HPLC analysis of the degradation products of cumene hydroperoxide

WT and E113Q MauG (10 μM) was individually mixed with cumene hydroperoxide (250 μM). The reaction mixture was then incubated on ice for 4 h. This long incubation period was needed because cumene hydroperoxide is a sluggish reactant to MauG. The reaction was terminated by removing the protein with an Amicon Ultra centrifugal filter unit (0.5 mL volume, 10 kDa nominal molecular weight limit). Aliquots of the protein-free fraction was analyzed using an Agilent 1200 HPLC system coupled with a C18 reverse-phase column. The column was initially equilibrated with 15% acetonitrile in water. After sample injection, a gradient elution process (from 15% to 80% acetonitrile) was initiated at a flow rate of 1.5 mL/min. The UV absorbance of eluted components was monitored at 210 nm. Assignment of individual components on the HPLC chromatograms was performed based on comparison of their retention times with those of standard compounds, including cumene hydroperoxide, cumyl alcohol, and acetophenone. Phenethyl alcohol (250 μM) was used as an internal standard for quantitative analysis. It was added to the protein-free fraction prior to the HPLC analysis. All HPLC measurements were performed in triplicate.

3. Results and discussion

3.1. Sequence alignment and structural analysis

Fig. 3 shows the result of our sequence alignment analysis on the bCcP superfamily, including MauG and bCcP from different organisms. It is evident that Glu113 is highly conserved in MauG. More importantly, it is located in a position that is analogous to the position of the aforementioned glutamate residue that functions as an acid-base catalyst during the activation of H_2O_2 in bCcP (Fig. 4). An asparagine residue, Asn110, is also highly conserved in MauG (Fig. 3) and forms an H-bonding interaction with Glu113 (Fig. 4A). This asparagine residue is

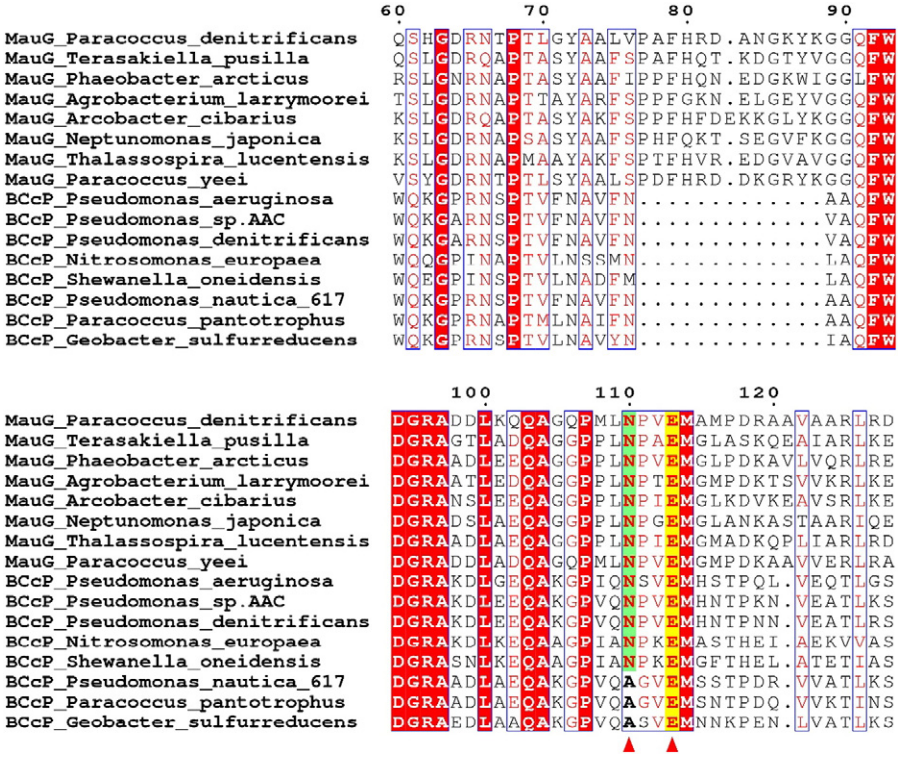

Fig. 3. Sequence alignment of the bCcP superfamily. Highly conserved residues are shown with red text and boxed in blue; strictly conserved residues are shown in a red background; the conserved glutamate residue located at the distal pocket of Heme$_{5C}$ is highlighted in a yellow background; the asparagine residue that is H-bonded to the conserved glutamate residue is shown in a green background.

proposed to optimize the physical position and orientation of Glu113 for H_2O_2 activation. A similar asparagine residue is present in some bCcPs but is not strictly conserved (Figs. 3 and 4).

It should be noted that another member of the bCcP superfamily, rubber oxygenase A (RoxA) [23], does not contain a corresponding glutamate residue in the distal pocket of Heme$_{5C}$ (Fig. 4D). A phenylalanine

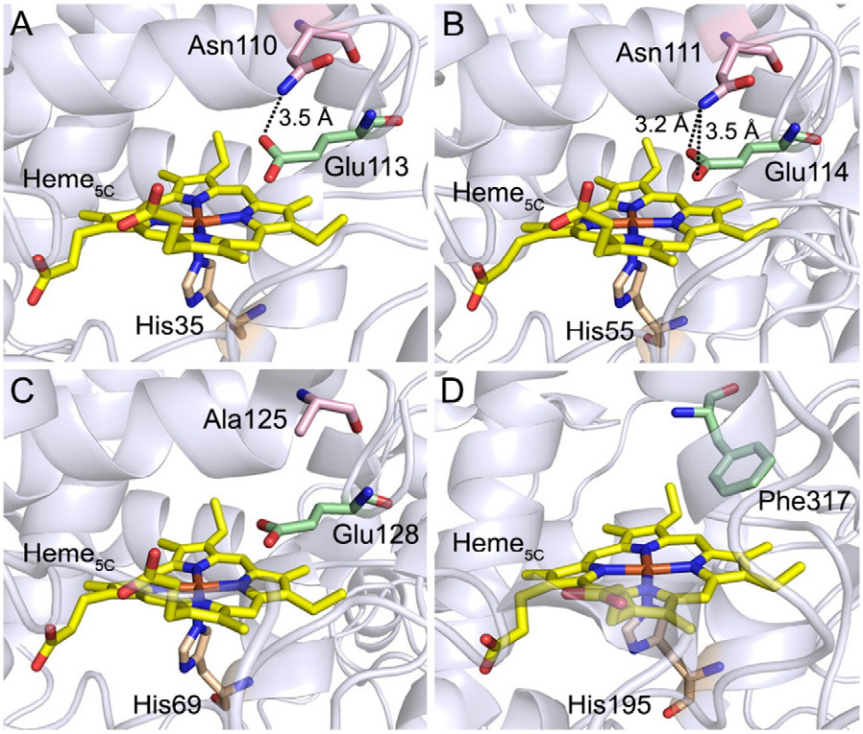

Fig. 4. Structural comparison of the Heme$_{5C}$ sites of (A) *Paracoccus denitrificans* MauG (PDB entry: 3L4M), (B) *Pseudomonas aeruginosa* bCcP (PDB entry: 2VHD), (C) *Paracoccus pantotrophus* bCcP (PDB entry: 2C1V), and (D) *Xanthomonas* sp. RoxA (PDB entry: 4B2N). The heme cofactor and key residues in the heme pocket are shown as sticks. The protein matrix is shown as cartoons in blue white.

residue occupies the corresponding position. Interestingly, RoxA is the only member in the bCcP superfamily that utilizes molecular oxygen instead of H_2O_2 as the oxidizing agent [23,25]. Thus, it is not surprising that the corresponding glutamate residue is absent in the distal pocket of $Heme_{5C}$ in RoxA as the reaction is completely different from those catalyzed by other enzymes in the bCcP superfamily. Table 1 summarizes the acid-base catalytic residues for heterolytic O—O bond cleavage and their interacting partners in the bCcP superfamily and other H_2O_2-utilizing hemoenzymes.

3.2. EPR characterization of the redox reactions of MauG

Fig. 5 shows the EPR spectra of WT and E113Q MauG. The EPR spectrum of diferric WT MauG reveals the presence of three ferric heme species: a high-spin heme at $g = 5.57$ and 2.00 ($Heme_{5C}$, $S = 5/2$), a major low-spin heme at $g = 2.54$, 2.19, and 1.87 ($Heme_{6C}$, $S = 1/2$), and a minor low-spin heme at $g = 2.89$, 2.32, and 1.52 ($S = 1/2$), which was previously attributed to a freezing-induced artifact originating from a minor fraction of the high-spin $Heme_{5C}$ species (Fig. 5A, black trace) [29,32,39]. The identity of this freezing-induced artifact is assigned as a hydroxide-bound hexacoordinate low-spin $Heme_{5C}$ species, based on the similarity of its *g*-values to those of the hydroxide-bound hexacoordinate low-spin heme species reported in other hemoproteins [40,41]. The hydroxide ligand is believed to be derived from a $Heme_{5C}$-bound water molecule shown in the crystal structure of MauG [22]. This EPR spectral assignment is further supported by our previous Mössbauer data [29,39] and by the fact that the freezing-induced low-spin species is completely absent in P107S MauG, a mutant in which the sixth coordination position of $Heme_{5C}$ is occupied by Glu113 [42]. In P107S MauG, the heme-bound Glu113 residue cannot be readily replaced by a solvent molecule and hence the minor low-spin species at $g = 2.89$, 2.32, and 1.52 cannot be observed.

Addition of an excess amount of dithionite to diferric MauG caused simultaneous reduction of both hemes, generating an EPR-silent diferrous species (Fig. 5A, blue trace). Upon addition of a stoichiometric amount of H_2O_2 to diferric MauG, the *bis*-Fe(IV) species was produced [29], and a substantial decrease in the EPR signals of both $Heme_{5C}$ and $Heme_{6C}$ was observed (Fig. 5A, green trace). Our previous Mössbauer study showed that there is no Fe(II) species in the diferric MauG samples treated with H_2O_2 [29]. Therefore, the observed decrease in the EPR signal upon addition of H_2O_2 to the diferric MauG sample was solely caused by the formation of Fe(IV) species. Given that the heme concentration was kept the same among different samples and that the EPR measurement condition remained unaltered, we were able to quantify the percentage decrease of the Fe(III) species caused by the reaction with H_2O_2. The percentage decrease of the Fe(III) species corresponded to the percentage formation of the Fe(IV) species. The high-spin signal ($Heme_{5C}$) decreased to ca. 13% of its original intensity, and the major low-spin signal ($Heme_{6C}$) decreased to ca. 25% of its original intensity, suggesting that the percentage of Fe(IV) was ca. 87% and 75% for $Heme_{5C}$ and $Heme_{6C}$, respectively. As summarized in Table 2, this H_2O_2-treated MauG sample was composed of (1) the *bis*-Fe(IV) species (75.0%), (2) the diferric species (13.1%), and (3) a mixed-valence Fe(IV)/Fe(III) ($Heme_{5C}$/$Heme_{6C}$) species (11.9%). The diferric species might be composed of unreacted protein and the decay product of the *bis*-Fe(IV) species. The mixed-valence species was generated possibly via homolytic cleavage of the O—O bond of H_2O_2, which allowed the incorporation of only one oxidizing equivalent to the diheme system of MauG. A portion of the mixed-valence species might be a decay intermediate of the *bis*-Fe(IV) species with one oxidizing equivalent retained in the diheme system and the other oxidizing equivalent translocated elsewhere [29]. Nonetheless, the ratio between heterolytic and homolytic O—O bond cleavage was close to 6.3 for WT MauG (Table 2).

Mutation of Glu113 to a glutamine eliminated the minor low-spin ferric species from the EPR spectrum and caused an increase in the EPR signal of the high-spin $Heme_{5C}$ species (Fig. 5B, black trace). The observation further confirms our aforementioned assignment of the minor low-spin species as a derivative of the high-spin $Heme_{5C}$ species. The crystal structure of WT MauG shows that Glu113 forms an H-bonding interaction with the $Heme_{5C}$-bound water molecule by serving as an H-bond acceptor [22]. During the sample freezing process, the $Heme_{5C}$-bound water molecule might become deprotonated with Glu113 as a proton acceptor, thereby generating the hydroxide-bound hexacoordinate $Heme_{5C}$ species in the WT enzyme. Due to the fact that hydroxide is a stronger field ligand than water for the heme iron, spin transition can be triggered upon deprotonation of the $Heme_{5C}$-bound water molecule, thereby rendering the hydroxide-bound hexacoordinate $Heme_{5C}$ species to be in a low-spin state. In the E113Q variant, the Gln113 residue can potentially maintain the H-bonding interaction with the $Heme_{5C}$-bound water molecule but cannot serve as a proton acceptor. Therefore, the hydroxide-bound low-spin $Heme_{5C}$ species cannot be generated during the sample freezing process. Addition of an excess amount of dithionite to diferric E113Q MauG led to reduction of $Heme_{5C}$ as the high-spin EPR signal completely disappeared (Fig. 5B, blue trace). However, the low-spin EPR signal remained unchanged, suggesting that an Fe(II)/Fe(III) ($Heme_{5C}$/$Heme_{6C}$) mixed-valence species was present in the dithionite-treated EPR sample. This result indicates that electron transfer from $Heme_{5C}$ to $Heme_{6C}$ was inhibited

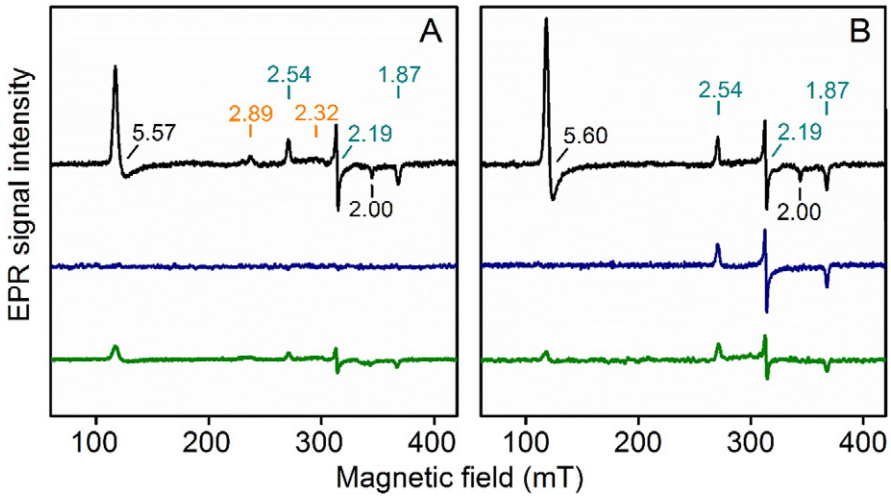

Fig. 5. EPR spectra of (A) WT and (B) E113Q MauG. Black: diferric MauG; blue: diferric MauG + ten eq. sodium dithionite; green: diferric MauG + one eq. H_2O_2. The *g* values of the EPR signals are labelled.

Table 2
The ratios of heterolytic O—O bond cleavage to homolytic O—O bond cleavage in WT and E113Q MauG.

	EPR study (hydrogen peroxide)					HPLC study (cumene hydroperoxide)		
	bis-Fe(IV) (heterolytic)[a]	Fe(IV)/Fe(III) (homolytic)	Ratio (hetero/homo)	Chance of heterolytic cleavage	Chance of a successful turnover[b]	Cumyl alcohol (heterolytic)	Acetophenone (homolytic)	Ratio (hetero/homo)
WT	75.0 (4.7) %[c]	11.9 (0.7) %	6.3	86%	64%	85.1 (0.3) %	14.9 (0.4) %	5.7
E113Q	53.8 (3.3) %	41.4 (2.6) %	1.3	57%	18%	74.9 (0.4) %	25.1 (0.7) %	3.0

[a] Note that the *bis*-Fe(IV) species and the Fe(IV)/Fe(III) mixed-valance species did not account for 100% of the enzyme because there was a small portion of the enzyme in the diferric state.
[b] A complete turnover of MauG takes three rounds of H_2O_2-activation.
[c] The numbers in parentheses are standard errors.

upon mutation of Glu113. After adding a stoichiometric amount of H_2O_2 to diferric E113Q MauG, the high-spin signal decreased to ca. 5% of its original intensity, and the low-spin signal decreased to ca. 46% of its original intensity (Fig. 5B, green trace), suggesting that the percentage of Fe(IV) was ca. 95% and 54% for $Heme_{5C}$ and $Heme_{6C}$, respectively. As shown in Table 2, this H_2O_2-treated E113Q MauG sample was composed of (1) the *bis*-Fe(IV) species (53.8%), (2) the diferric species (4.8%), and (3) the mixed-valence Fe(IV)/Fe(III) ($Heme_{5C}$/$Heme_{6C}$) species (41.4%). The ratio between heterolytic and homolytic O—O bond cleavage was ca. 1.3 for E113Q MauG (Table 2). Therefore, it is evident that mutation of Glu113 caused a significant increase in the percentage of the mixed-valence Fe(IV)/Fe(III) species, revealing the acid-base catalytic role of Glu113 in facilitating heterolytic cleavage of the O—O bond of H_2O_2.

3.3. HPLC study of the degradation products of cumene hydroperoxide

In order to further examine the effect of Glu113 on the O—O bond cleavage pattern, we performed reactions of WT and E113Q MauG with cumene hydroperoxide. As shown in Fig. S1, heterolytic cleavage of the O—O bond of cumene hydroperoxide by ferric hemoproteins leads to the production of compound I (chemically equivalent to the *bis*-Fe(IV) species of MauG) and cumyl alcohol, whereas homolytic cleavage of the O—O bond generates compound II (chemically equivalent to the oxidized mixed-valence species of MauG, i.e., Fe(IV)/Fe(III) ($Heme_{5C}$/$Heme_{6C}$)) and $PhC(CH_3)_2O\bullet$, which subsequently decays to acetophenone via the release of a methyl radical [43–46]. The degradation products of cumene hydroperoxide in reactions with WT and E113Q MauG were analyzed by HPLC using a reverse-phase C18 column. Cumene hydroperoxide was eluted at 9.7 min and the internal standard, phenethyl alcohol, was eluted at 6.9 min; the two degradation products of cumene hydroperoxide, cumyl alcohol and acetophenone, were eluted at 8.3 min and 8.8 min, respectively (Fig. S2).

The reaction between cumene hydroperoxide and WT MauG caused degradation of cumene hydroperoxide and simultaneous formation of both cumyl alcohol and acetophenone (Fig. S2). No other degradation products of cumene hydroperoxide were identified (Fig. S2). At the HPLC signal detection wavelength, i.e., 210 nm, cumyl alcohol and acetophenone have almost the same molar absorptivity. A comparison of the peak areas of these two products revealed a ratio of 5.7 between cumyl alcohol and acetophenone, suggesting that the ratio between heterolytic and homolytic O—O bond cleavage catalyzed by WT MauG was 5.7 (Table 2). In the reaction between cumene hydroperoxide and E113Q MauG, this ratio was decreased to 3.0 (Table 2). Thus, the mutation of Glu113 inhibited heterolytic O—O bond cleavage and promoted homolytic O—O bond cleavage, consistent with the EPR result. Notably, the ratios between heterolytic and homolytic O—O bond cleavage determined by the HPLC experiments were not the same as those determined by the EPR experiments, despite exhibiting the same trend of change following the mutation of Glu113. This observed inconsistency in the ratios from these two sets of experiments might be caused by the difference in the chemical structures of the peroxides used in the studies. Compared to hydrogen peroxide, cumene hydroperoxide contains a bulky substitution group, which may facilitate a different binding conformation in the $Heme_{5C}$ site of MauG, thereby altering the process of O—O bond cleavage and causing a change in the hetero/homo ratio.

3.4. Comments on the catalytic role of Glu113

Fig. 6 summarizes the redox events that occurred to WT MauG and the E113Q mutant in this study. Based on our results, we conclude that Glu113 plays a structural and electronic role in controlling the reactivity of $Heme_{5C}$. In the resting diferric state, Glu113 forms an H-bonding interaction with the $Heme_{5C}$-bound water molecule and makes it a stronger field ligand to the heme iron (Fig. 6). This interaction may help to stabilize $Heme_{5C}$ and prevent it from non-productive binding and redox events. In WT MauG, the two hemes share electrons efficiently, despite being physically separated [34]. They exhibit redox cooperativity and behave as a single diheme unit rather than as independent hemes [47]. The mutation of Glu113 disrupted the redox equilibrium between the two hemes and cut off electron transfer from $Heme_{5C}$ to $Heme_{6C}$. As a result, addition of dithionite to diferric E113Q MauG generated the reduced mixed-valence species, i.e., Fe(II)/Fe(III) ($Heme_{5C}$/$Heme_{6C}$), which had never been observed in WT MauG or other MauG mutants under similar reaction conditions (Fig. 6) [47].

During the reaction with H_2O_2, Glu113 facilitates the activation of H_2O_2 by functioning as an acid-base catalyst to drive the heterolytic O—O bond cleavage that is critical for *bis*-Fe(IV) formation (Fig. 6). The presence of Glu113 in WT MauG enabled heterolytic O—O bond cleavage to be the dominating reaction pathway. It is believed that binding of the primary substrate of MauG, preMADH, may trigger conformation changes that further promote heterolytic O—O bond cleavage by improving the catalytic efficiency of Glu113. In E113Q MauG, there were similar probabilities for homolytic O—O bond cleavage and heterolytic O—O bond cleavage to occur during the reaction with H_2O_2 in the absence of preMADH (Table 2). The former scenario led to production of the Fe(IV)/Fe(III) ($Heme_{5C}$/$Heme_{6C}$) mixed-valence species and a hydroxyl radical, and the latter resulted in generation of the *bis*-Fe(IV) species (Fig. 6).

3.5. Comments on the catalytic behavior of E113Q MauG

Interestingly, previous studies on the E113Q mutant revealed some surprising catalytic behaviors: it displayed no detectable TTQ biosynthesis activity in aqueous solution under steady-state reaction conditions, but X-ray crystallographic studies showed that this mutant achieved partial synthesis of TTQ from *in crystallo* reactions, in which H_2O_2 was added to the co-crystals of the E113Q MauG-preMADH complex [35] Extended exposure of these crystals to H_2O_2 resulted in hydroxylation of Pro107 in the distal pocket of $Heme_{5C}$ [35]. Herein, our results provide a reasonable explanation for the abnormal activity of this mutant. In E113Q MauG, each round of H_2O_2 activation has a ca. 43% chance to generate the Fe(IV)/Fe(III) ($Heme_{5C}$/$Heme_{6C}$) mixed-valence species via homolytic O—O bond cleavage (Table 2). Although this number may vary in cases when the primary substrate, preMADH, is bound to E113Q MauG prior to the binding event of H_2O_2, the probability of homolytic O—O bond cleavage is increased in this mutant compared to the WT enzyme. It is unclear whether the Fe(IV)/Fe(III) mixed-valence

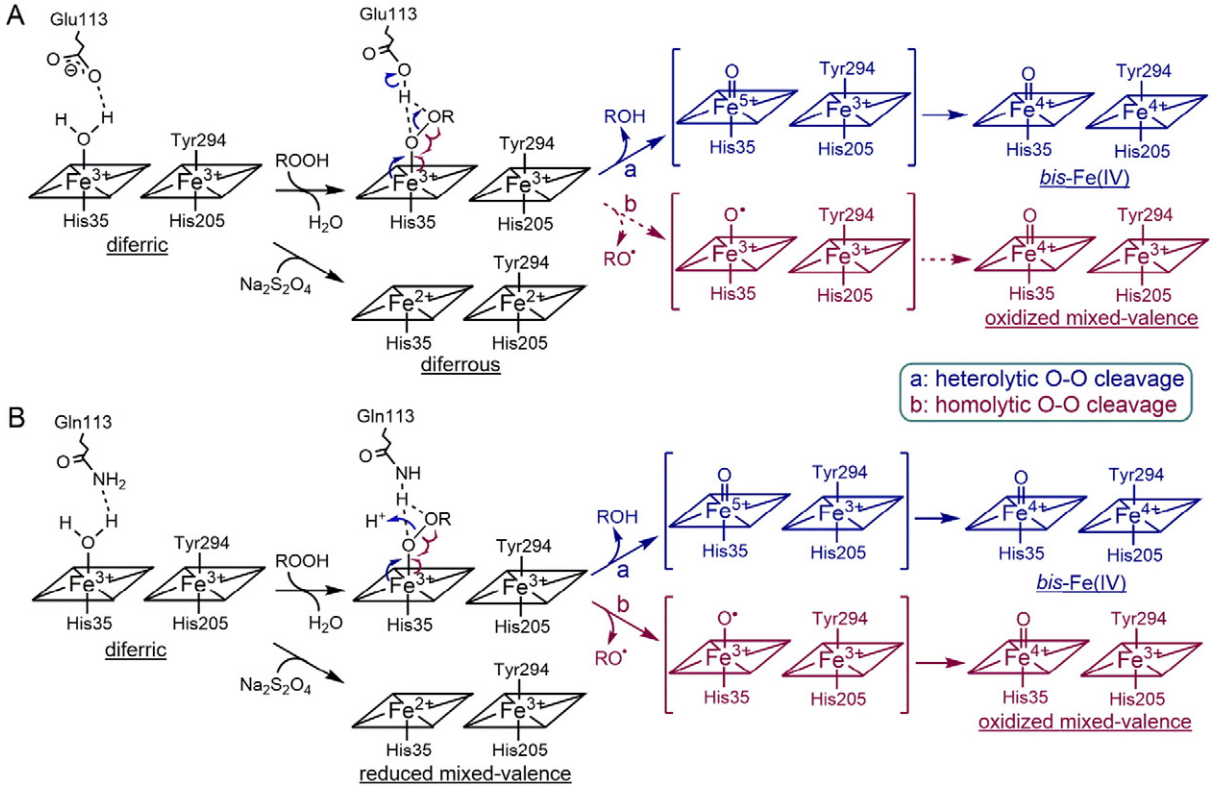

Fig. 6. Redox events of (A) WT MauG and (B) E113Q MauG. Different redox states revealed from the EPR study are illustrated. In WT MauG the pathway "a" is the dominating reaction pathway, whereas in E113Q MauG the two pathways have similar possibilities to occur.

species is capable of remotely oxidizing preMADH. Nonetheless, the overall TTQ biosynthesis is expected to be hampered in E113Q MauG because of the uncoupling of the two oxidizing equivalents and the oxidative damage caused by the non-productive hydroxyl radical generated as a result of homolytic O—O bond cleavage.

As shown in Fig. 2B, a complete cycle of TTQ biosynthesis requires three rounds of H_2O_2 activation, and the *bis*-Fe(IV) species is generated in each round and subsequently consumed to complete one of the three consecutive two-electron oxidation steps on preMADH [25,27]. In fact, this unique nature of the MauG-catalyzed reaction (i.e., multiple rounds of H_2O_2 activation are required for each turnover) pronouncedly magnified the effect of the Glu-to-Gln mutation on the success rate of the overall reaction. As shown in Table 2, with a homolytic O—O cleavage rate at 43%, the probability of a successful MauG turnover is calculated to be only 18%. Therefore, it was possible for E113Q MauG to catalyze limited rounds of productive H_2O_2 activation, resulting in partial TTQ biosynthesis from *in crystallo* reactions. During these *in crystallo* reactions, the dissociation of the protein complex was inhibited, thereby allowing the visualization of the chemical modifications on preMADH. In contrast, the E113Q mutant was incapable of multiple turnovers in aqueous solution under steady-state conditions. After several rounds of H_2O_2 activation, E113Q MauG would eventually become oxidatively modified around the $Heme_{5C}$ site and thus lose activity because of the inevitable homolytic O—O bond cleavage.

Acknowledgements

The financial support of this work was provided by the National Institutes of Health (grant number GM108988 to A.L.). We thank Dr. Victor Davidson for providing us with the expression system of MauG. J.G. acknowledges the William M. Suttles doctoral research fellowship and the doctoral dissertation grant from Georgia State University as well as the American Heart Association Postdoctoral Fellowship. J.G. and L.H. acknowledge the Molecular Basis of Disease graduate fellowship from Georgia State University. A.L. acknowledges the Lutcher Brown Endowment Fund for the research support.

Appendix A. Supplementary data

Supplementary data to this article can be found online at http://dx.doi.org/10.1016/j.jinorgbio.2016.11.013.

References

[1] C.C. Winterbourn, The biological chemistry of hydrogen peroxide, Methods Enzymol. 528 (2013) 3–25.
[2] E.A. Veal, A.M. Day, B.A. Morgan, Hydrogen peroxide sensing and signaling, Mol. Cell 26 (2007) 1–14.
[3] M. Giorgio, M. Trinei, E. Migliaccio, P.G. Pelicci, Hydrogen peroxide: a metabolic by-product or a common mediator of ageing signals? Nat. Rev. Mol. Cell Biol. 8 (2007) 722–728.
[4] M. Sono, M.P. Roach, E.D. Coulter, J.H. Dawson, Heme-containing oxygenases, Chem. Rev. 96 (1996) 2841–2888.
[5] T.L. Poulos, Heme enzyme structure and function, Chem. Rev. 114 (2014) 3919–3962.
[6] I. Matsunaga, Y. Shiro, Peroxide-utilizing biocatalysts: structural and functional diversity of heme-containing enzymes, Curr. Opin. Chem. Biol. 8 (2004) 127–132.
[7] T.P. Ko, M.K. Safo, F.N. Musayev, M.L. Di Salvo, C. Wang, S.H. Wu, D.J. Abraham, Structure of human erythrocyte catalase, Acta Crystallogr. D Biol. Crystallogr. 56 (2000) 241–245.
[8] B.C. Finzel, T.L. Poulos, J. Kraut, Crystal structure of yeast cytochrome *c* peroxidase refined at 1.7-Å resolution, J. Biol. Chem. 259 (1984) 13027–13036.
[9] M. Gajhede, D.J. Schuller, A. Henriksen, A.T. Smith, T.L. Poulos, Crystal structure of horseradish peroxidase C at 2.15 angstrom resolution, Nat. Struct. Biol. 4 (1997) 1032–1038.
[10] W.R. Patterson, T.L. Poulos, Crystal structure of recombinant pea cytosolic ascorbate peroxidase, Biochemistry 34 (1995) 4331–4341.
[11] T.L. Poulos, S.T. Freer, R.A. Alden, S.L. Edwards, U. Skogland, K. Takio, B. Eriksson, N. Xuong, T. Yonetani, J. Kraut, The crystal structure of cytochrome *c* peroxidase, J. Biol. Chem. 255 (1980) 575–580.
[12] X. Carpena, S. Loprasert, S. Mongkolsuk, J. Switala, P.C. Loewen, I. Fita, Catalase-peroxidase KatG of *Burkholderia pseudomallei* at 1.7 Å resolution, J. Mol. Biol. 327 (2003) 475–489.

[13] M.G. Malkowski, S.L. Ginell, W.L. Smith, R.M. Garavito, The productive conformation of arachidonic acid bound to prostaglandin synthase, Science 289 (2000) 1933–1937.
[14] M. Hofrichter, R. Ullrich, Oxidations catalyzed by fungal peroxygenases, Curr. Opin. Chem. Biol. 19 (2014) 116–125.
[15] K. Piontek, E. Strittmatter, R. Ullrich, G. Grobe, M.J. Pecyna, M. Kluge, K. Scheibner, M. Hofrichter, D.A. Plattner, Structural basis of substrate conversion in a new aromatic peroxygenase: cytochrome P450 functionality with benefits, J. Biol. Chem. 288 (2013) 34767–34776.
[16] M. Sundaramoorthy, J. Terner, T.L. Poulos, The crystal structure of chloroperoxidase: a heme peroxidase-cytochrome P450 functional hybrid, Structure 3 (1995) 1367–1377.
[17] A. Echalier, T. Brittain, J. Wright, S. Boycheva, G.B. Mortuza, V. Fulop, N.J. Watmough, Redox-linked structural changes associated with the formation of a catalytically competent form of the diheme cytochrome *c* peroxidase from *Pseudomonas aeruginosa*, Biochemistry 47 (2008) 1947–1956.
[18] D.S. Lee, A. Yamada, H. Sugimoto, I. Matsunaga, H. Ogura, K. Ichihara, S. Adachi, S.Y. Park, Y. Shiro, Substrate recognition and molecular mechanism of fatty acid hydroxylation by cytochrome P450 from *Bacillus subtilis*. Crystallographic, spectroscopic, and mutational studies, J. Biol. Chem. 278 (2003) 9761–9767.
[19] R. Singh, J.C. Grigg, Z. Armstrong, M.E. Murphy, L.D. Eltis, Distal heme pocket residues of B-type dye-decolorizing peroxidase: arginine but not aspartate is essential for peroxidase activity, J. Biol. Chem. 287 (2012) 10623–10630.
[20] Y. Sugano, R. Muramatsu, A. Ichiyanagi, T. Sato, M. Shoda, DyP, a unique dye-decolorizing peroxidase, represents a novel heme peroxidase family: ASP171 replaces the distal histidine of classical peroxidases, J. Biol. Chem. 282 (2007) 36652–36658.
[21] T. Yoshida, H. Tsuge, H. Konno, T. Hisabori, Y. Sugano, The catalytic mechanism of dye-decolorizing peroxidase DyP may require the swinging movement of an aspartic acid residue, FEBS J. 278 (2011) 2387–2394.
[22] L.M.R. Jensen, R. Sanishvili, V.L. Davidson, C.M. Wilmot, In crystallosposttranslational modification within a MauG/pre-methylamine dehydrogenase complex, Science 327 (2010) 1392–1394.
[23] J. Seidel, G. Schmitt, M. Hoffmann, D. Jendrossek, O. Einsle, Structure of the processive rubber oxygenase RoxA from *Xanthomonas* sp. Proc. Natl. Acad. Sci. U. S. A. 110 (2013) 13833–13838.
[24] Y. Wang, M.E. Graichen, A. Liu, A.R. Pearson, C.M. Wilmot, V.L. Davidson, MauG, a novel diheme protein required for tryptophan tryptophylquinone biogenesis, Biochemistry 42 (2003) 7318–7325.
[25] J. Geng, I. Davis, F. Liu, A. Liu, Bis-Fe(IV): nature's sniper for long-range oxidation, J. Biol. Inorg. Chem. 19 (2014) 1057–1067.
[26] V.L. Davidson, A. Liu, Tryptophan tryptophylquinone biosynthesis: a radical approach to posttranslational modification, Biochim. Biophys. Acta 1824 (2012) 1299–1305.
[27] E.T. Yukl, F. Liu, J. Krzystek, S. Shin, L.M.R. Jensen, V.L. Davidson, C.M. Wilmot, A. Liu, Diradical intermediate within the context of tryptophan tryptophylquinone biosynthesis, Proc. Natl. Acad. Sci. U. S. A. 110 (2013) 4569–4573.
[28] N. Abu Tarboush, L.M. Jensen, E.T. Yukl, J. Geng, A. Liu, C.M. Wilmot, V.L. Davidson, Mutagenesis of tryptophan199 suggests that hopping is required for MauG-dependent tryptophan tryptophylquinone biosynthesis, Proc. Natl. Acad. Sci. U. S. A. 108 (2011) 16956–16961.
[29] X. Li, R. Fu, S. Lee, C. Krebs, V.L. Davidson, A. Liu, A catalytic di-heme bis-Fe(IV) intermediate, alternative to an Fe(IV)═O porphyrin radical, Proc. Natl. Acad. Sci. U. S. A. 105 (2008) 8597–8600.
[30] J. Geng, K. Dornevil, V.L. Davidson, A. Liu, Tryptophan-mediated charge-resonance stabilization in the bis-Fe(IV) redox state of MauG, Proc. Natl. Acad. Sci. U. S. A. 110 (2013) 9639–9644.
[31] J. Geng, I. Davis, A. Liu, Probing bis-Fe(IV) MauG: experimental evidence for the long-range charge-resonance model, Angew. Chem. Int. Ed. 54 (2015) 3692–3696.
[32] N. Abu Tarboush, S. Shin, J. Geng, A. Liu, V.L. Davidson, Effects of the loss of the axial tyrosine ligand of the low-spin heme of MauG on its physical properties and reactivity, FEBS Lett. 586 (2012) 4339–4343.
[33] S. Lee, S. Shin, X. Li, V.L. Davidson, Kinetic mechanism for the initial steps in MauG-dependent tryptophan tryptophylquinone biosynthesis, Biochemistry 48 (2009) 2442–2447.
[34] R. Fu, F. Liu, V.L. Davidson, A. Liu, Heme iron nitrosyl complex of MauG reveals an efficient redox equilibrium between hemes with only one heme exclusively binding exogenous ligands, Biochemistry 48 (2009) 11603–11605.
[35] N. Abu Tarboush, E.T. Yukl, S. Shin, M. Feng, C.M. Wilmot, V.L. Davidson, Carboxyl group of Glu113 is required for stabilization of the diferrous and bis-Fe(IV) states of MauG, Biochemistry 52 (2013) 6358–6367.
[36] P. Gouet, X. Robert, E. Courcelle, ESPript/ENDscript: extracting and rendering sequence and 3D information from atomic structures of proteins, Nucleic Acids Res. 31 (2003) 3320–3323.
[37] R. Fu, R. Gupta, J. Geng, K. Dornevil, S. Wang, Y. Zhang, M.P. Hendrich, A. Liu, Enzyme reactivation by hydrogen peroxide in heme-based tryptophan dioxygenase, J. Biol. Chem. 286 (2011) 26541–26554.
[38] J. Beltran, B. Kloss, J.P. Hosler, J.F. Geng, A.M. Liu, A. Modi, J.H. Dawson, M. Sono, M. Shumskaya, C. Ampomah-Dwamena, J.D. Love, E.T. Wurtzel, Control of carotenoid biosynthesis through a heme-based cis-trans isomerase, Nat. Chem. Biol. 11 (2015), 598-U104.
[39] Y. Chen, S.G. Naik, J. Krzystek, S. Shin, W.H. Nelson, S. Xue, J.J. Yang, V.L. Davidson, A. Liu, Role of calcium in metalloenzymes: effects of calcium removal on the axial ligation geometry and magnetic properties of the catalytic diheme center in MauG, Biochemistry 51 (2012) 1586–1597.
[40] J. Geng, K. Dornevil, A. Liu, Chemical rescue of the distal histidine mutants of tryptophan 2,3-dioxygenase, J. Am. Chem. Soc. 134 (2012) 12209–12218.
[41] T. Yonetani, H. Anni, Yeast cytochrome *c* peroxidase - coordination and spin states of heme prosthetic group, J. Biol. Chem. 262 (1987) 9547–9554.
[42] M. Feng, L.M.R. Jensen, E.T. Yukl, X. Wei, A. Liu, C.M. Wilmot, V.L. Davidson, Proline 107 is a major determinant in maintaining the structure of the distal pocket and reactivity of the high-spin heme of MauG, Biochemistry 51 (2012) 1598–1606.
[43] T. Shimizu, Y. Murakami, M. Hatano, Glu318 and Thr319 mutations of cytochrome P450 1A2 remarkably enhance homolytic O—O cleavage of alkyl hydroperoxides. An optical absorption spectral study, J. Biol. Chem. 269 (1994) 13296–13304.
[44] T. Matsui, S. Ozaki, E. Liong, G.N. Phillips Jr., Y. Watanabe, Effects of the location of distal histidine in the reaction of myoglobin with hydrogen peroxide, J. Biol. Chem. 274 (1999) 2838–2844.
[45] K. Hiroya, M. Ishigooka, T. Shimizu, M. Hatano, Role of Glu318 and Thr319 in the catalytic function of cytochrome P450d (P4501A2): effects of mutations on the methanol hydroxylation, FASEB J. 6 (1992) 749–751.
[46] S. Adachi, S. Nagano, K. Ishimori, Y. Watanabe, I. Morishima, T. Egawa, T. Kitagawa, R. Makino, Roles of proximal ligand in heme proteins: replacement of proximal histidine of human myoglobin with cysteine and tyrosine by site-directed mutagenesis as models for P-450, chloroperoxidase, and catalase, Biochemistry 32 (1993) 241–252.
[47] X. Li, M. Feng, Y. Wang, H. Tachikawa, V.L. Davidson, Evidence for redox cooperativity between *c*-type hemes of MauG which is likely coupled to oxygen activation during tryptophan tryptophylquinone biosynthesis, Biochemistry 45 (2006) 821–828.